Available online at website: https://journal.bcrec.id/index.php/bcrec

Bulletin of Chemical Reaction Engineering & Catalysis, 21 (2) 2026, 403-411

Original Research Article

Effect of Equimolar Sodium Borohydride-Ferric Chloride Concentrations on Nano Zero-Valent Iron/Palm Shell Composites for Simultaneous Nanogold Recovery and Hydrogen Generation

Puteri Nur Syakinah Nordin[1], Aina Syamimi Noor Helmy[1], Chan Juinn Chieh Derek[2], Mohd Fariz Rajuli[3], Siu Hua Chang[1]*

[1]*Waste Management and Resource Recovery (WeResCue) Group, Faculty of Chemical Engineering, Universiti Teknologi MARA, Cawangan Pulau Pinang, 13500 Permatang Pauh, Penang, Malaysia*
[2]*School of Chemical Engineering, Engineering Campus, Universiti Sains Malaysia, Seri Ampangan, 14300 Nibong Tebal, Seberang Perai Selatan, Pulau Pinang, Malaysia*
[3]*Petronas Gas Berhad Level 49-50, Tower 1, Petronas Twin Towers, 50088 Kuala Lumpur, Malaysia.*

Received: 13th January 2026; Revised: 19th February 2026; Accepted: 20th February 2026
Available online: 8th March 2026; Published regularly: August 2026

Abstract

Gold-containing waste solutions represent both an environmental liability and a valuable secondary resource, yet few existing technologies integrate nanogold recovery with sustainable hydrogen generation from these streams. In this study, the effect of equimolar sodium borohydride–ferric chloride ($NaBH_4$–$FeCl_3$) concentrations on the synthesis and performance of nanoscale zero-valent iron (nZVI)/palm shell composites was systematically investigated for the simultaneous recovery of nanogold and generation of hydrogen from gold-containing aqueous solutions. The composites were synthesized at different equimolar $NaBH_4$–$FeCl_3$ concentrations (0.5–2.0 M), while maintaining a fixed overall molar ratio, with palm shell biomass employed as a support to suppress particle aggregation and preserve reactive surface area. Nanogold formation was evaluated using UV–Vis spectroscopy via localized surface plasmon resonance, while hydrogen evolution was quantified by a water-displacement method. Surface properties were characterized by BET analysis. Nanogold recovery increased progressively with increasing equimolar precursor concentration, whereas hydrogen production exhibited a non-linear dependence, reaching a maximum of 29.02 mL at 1.5 M, which also corresponded to the highest BET surface area (13.57 m^2/g). Further increasing the equimolar $NaBH_4$–$FeCl_3$ concentration to 2.0 M led to surface passivation and diminished reactivity. These results demonstrate that equimolar precursor concentration plays a critical role in governing nZVI/palm shell composite structure and functionality. The optimized composite exhibits strong potential as a multifunctional material for integrated precious metal recovery and green hydrogen production, thereby contributing to sustainable circular resource utilization and clean energy technologies.

Keywords: Nano zero-valent iron; Equimolar precursor concentrations; Nanogold recovery; Hydrogen generation; Palm shell composites

How to Cite: Nordin, P.N.S., Helmy, A.S.N., Derek, C.J.C., Rajuli, M.F., Chang, S.H. (2026). Effect of Equimolar Sodium Borohydride-Ferric Chloride Concentrations on Nano Zero-Valent Iron/Palm Shell Composites for Simultaneous Nanogold Recovery and Hydrogen Generation. *Bulletin of Chemical Reaction Engineering & Catalysis*, 21 (2), 403-411. (DOI: 10.9767/bcrec.20636)

Permalink/DOI: https://doi.org/10.9767/bcrec.20636

1. Introduction

Nanogold, valued for its size-dependent electrical, catalytic, and surface properties, is widely used in electronics, catalysis, sensing, and biomedicine [1,2]. Although electronic waste and industrial effluents contain abundant gold-bearing precursors [3], the recovery and controlled synthesis of nanogold from these complex matrices remain challenging due to inefficiencies in existing extraction and reduction approaches [4]. Conventional nanogold synthesis methods also often depend on strong chemical reductants, hazardous solvents, and energy-intensive processes, raising both economic and

* Corresponding Author.
Email: shchang@uitm.edu.my (S. H. Chang)

environmental concerns [5–9]. In parallel, hydrogen has emerged as a clean and efficient energy carrier critical to achieving global carbon neutrality [10]. Although hydrogen can be produced via routes such as steam methane reforming, electrolysis, and biomass conversion [10,11], most conventional techniques are energy-intensive and generate substantial greenhouse gas emissions [12]. These challenges have intensified the search for cost-effective and eco-friendly nanogold recovery and hydrogen production technologies.

Recently, nanoscale zero-valent iron (nZVI) has attracted increasing attention as a multifunctional material for both nanogold recovery and hydrogen generation from aqueous systems, owing to its high reactivity, large specific surface area, cost effectiveness, and ability to function simultaneously as a reductant and an adsorbent [13]. Its characteristic core–shell structure, featuring a metallic Fe^0 core and an iron oxide shell, is widely proposed to support complementary reduction and sorption mechanisms. Specifically, the Fe° core generally considered to facilitate electron-transfer reactions, while the oxide shell provides adsorption sites that enhance reactant accessibility and stabilize reaction intermediates [14]. In nanogold recovery, nZVI has been reported to be capable of simultaneously reducing and adsorbing Au^{3+} ions from chloroauric acid ($HAuCl_4$) solutions to form elemental nanogold (Au^0), accompanied by oxidation of Fe^0 to Fe^{3+}, as described in Equation (1) [15,16]:

$$Fe^0 + AuCl_4^- \rightarrow Fe^{3+} + Au^0 + 4Cl^- \quad (1)$$

This coupled redox–sorption mechanism is commonly proposed as a simplified explanation for the efficient removal and immobilization of gold species on the nZVI surface without the use of toxic chemical reductants. Studies such as Li et al. [17] have reported high nanogold recovery efficiencies from industrial wastewater using nZVI, demonstrating its potential for sustainable resource reclamation. A similar redox–sorption interplay has also been proposed to contribute to hydrogen generation via water decomposition. In this process, the Fe^0 core is suggested to donate electrons to water molecules, producing hydrogen gas (H_2), while the oxide shell adsorbs and facilitates the dissociation of water at the solid–liquid interface, enhancing reaction kinetics [18]. The overall reaction is expressed in Equation (2) [18]:

$$3Fe^0 + 4H_2O \rightarrow Fe_3O_4 + 4H_2 \quad (2)$$

This pathway offers a conceptual route for hydrogen production without emitting greenhouse gases, unlike conventional thermochemical methods [19]. Although nZVI has been independently employed for nanogold recovery (Equation (1) and hydrogen production (Equation (2)), the integration of both processes within a single system has not been reported yet. The nZVI is typically synthesized through chemical reduction of ferric salts (e.g., $FeCl_3$) using strong reductants such as sodium borohydride ($NaBH_4$), as shown in Equation (3) [20].

$$2FeCl_3 + 6NaBH_4 + 18H_2O \rightarrow 2Fe^0 + 6NaCl + 6B(OH)_3 + 21H_2 \quad (3)$$

In this reaction, Fe^0 represents the reactive metallic core of nZVI responsible for reductive transformations. Theoretically, a $NaBH_4$:$FeCl_3$ molar ratio of 3:1 is required for complete reduction of Fe^{3+} to Fe^0. In practice, $NaBH_4$ is often used in excess to compensate for its rapid hydrolysis and other competing side reactions, thereby ensuring complete Fe^{3+} reduction [21]. However, excessively high $NaBH_4$:$FeCl_3$ ratios may induce uncontrolled hydrogen evolution, over-reduction, and the formation of boron-rich byproducts, which promote particle aggregation and surface passivation [21,22]. While the $NaBH_4$:$FeCl_3$ molar ratio governs the stoichiometric balance of the redox reaction, the absolute concentrations of both reagents play a critical role in influencing Fe^{3+} reduction kinetics, as well as nZVI nucleation, particle growth, and colloidal stability [23]. Our previous work identified a $NaBH_4$:$FeCl_3$ molar ratio of 4:1, slightly above the stoichiometric 3:1 requirement, as optimal for efficient and controlled nZVI formation [24]. Nevertheless, the influence of absolute reagent concentrations at this fixed optimal ratio remains unexplored. Importantly, varying reagent concentrations while maintaining equimolar $NaBH_4$ and $FeCl_3$ solutions and a constant overall 4:1 molar ratio enables isolation of concentration-dependent effects on Fe^{3+} reduction efficiency and nZVI yield, without interference from changes in molar ratio or total reagent volume. Such effects cannot be captured through molar-ratio adjustments alone, which primarily alter reaction stoichiometry rather than the physicochemical environment governing nZVI formation.

Accordingly, this study investigated the effect of varying the absolute concentrations of equimolar $NaBH_4$-$FeCl_3$ solutions, combined to maintain an overall $NaBH_4$:$FeCl_3$ molar ratio of 4:1, on nZVI yield and its performance in simultaneous nanogold recovery and hydrogen generation from gold-containing aqueous media. Palm shell, an abundant biomass in Malaysia [25], was employed as a support material to fabricate nZVI/palm shell composites, mitigating nZVI aggregation and preserving its reactive surface area. Nanogold recovery was quantified by

UV–Vis spectroscopy based on localized surface plasmon resonance (LSPR) intensity. Hydrogen production was measured via the water-displacement method, while the purity of the generated hydrogen gas was analysed using gas chromatography equipped with a flame ionisation detector (GC-FID). The surface properties and reactivity of the synthesized composites were further evaluated via Brunauer–Emmett–Teller (BET) analysis. Overall, this work provides fundamental insights into the role of reagent concentration in governing nZVI formation and offers enhanced control over nZVI composite reactivity for sustainable metal recovery and green hydrogen production.

2. Materials and Method

2.1 Materials

Iron(III) chloride hexahydrate ($FeCl_3 \cdot 6H_2O$, ≥99%), ethanol (C_2H_5OH, 99.7%v/v), and poly(vinyl alcohol) (PVA, ≥99%, fully hydrolyzed, viscosity 11.6–15.4 cps) were purchased from R&M Chemicals. Sodium borohydride ($NaBH_4$, ≥98%) was obtained from Bellamy Precision, while chloroauric acid ($HAuCl_4 \cdot 3H_2O$, ≥99.9%) was supplied by Sigma-Aldrich. Deionized water (resistivity 18.2 MΩ·cm) was used throughout all experiments. Palm shells were collected from a local palm oil mill, thoroughly washed with deionized water, dried at 80 °C for 24 h, and ground to a fine powder before use. All chemicals were used as received without further purification.

2.2. Fabrication of nZVI/Palm Shell Composites

The nZVI/palm shell composites were fabricated using a modified co-precipitation-reduction method under an inert nitrogen atmosphere, adapted from a previously reported method [26]. The raw palm shell biomass was washed, dried in an oven, ground, and sieved to a powder size of <65 μm. For each experiment, equimolar solutions of $FeCl_3$and $NaBH_4$with final concentrations of 0.5, 1.0, 1.25, and 1.5 M were prepared by dissolving the corresponding masses of ferric chloride hexahydrate ($FeCl_3 \cdot 6H_2O$) and sodium borohydride ($NaBH_4$) directly into their respective solvents, while maintaining consistent solution volumes and molar ratios across all conditions. The reagents ($FeCl_3 . 6H_2O$) were premixed with a 4:1 ethanol-water mixture (10 mL ethanol + 2.5 mL deionized water). This solution was mixed with 0.01 g of the palm shell powder in a round-bottom flask and stirred magnetically for 30 minutes to ensure uniform adsorption of iron onto the biomass. Subsequently, 55 mL of the corresponding equimolar concentration $NaBH_4$ solution was added to the suspension dropwise (~20 drops/min) to the $FeCl_3$/palm shell suspension under continuous stirring at 700 rpm. The addition of $NaBH_4$ initiated an immediate reduction reaction, evidenced by the appearance of a black precipitate upon the first drop. The reaction was allowed to proceed for 1 hour at room temperature to ensure complete reduction. Following the reaction, the black iron nanoparticles were separated from the solution using the centrifuge at 6000 rpm for 7 minutes. Thereafter, the collected precipitate was washed three times with ethanol and dried for 4 hours in a freeze dryer for further use and characterization.

2.3. Preparation of Gold-containing Solutions

A gold-containing solution was prepared to evaluate the nanogold recovery and concurrent hydrogen production performance of the synthesized nZVI/palm shell composites. Specifically, a 0.8 mM $HAuCl_4$ solution was prepared by appropriately diluting the liquid $HAuCl_4$ stock in 45 mL of deionized water under gentle stirring at room temperature. Subsequently, 5 mL of 2% (w/w) polyvinyl alcohol (PVA) solution was added as a stabilizing agent and mixed thoroughly. The pH of the gold-containing solution was then adjusted to 2.0 using 1 M HCl or 1 M NaOH, added dropwise with continuous stirring to ensure homogeneity, and the pH was monitored using a calibrated pH meter. Once the desired pH was attained, the solution was used immediately in the nanogold recovery and hydrogen generation experiments with nZVI/palm shell composites.

2.4. Recovery of Nanogold and Hydrogen Gas Collection

The procedure for simultaneous nanogold recovery and hydrogen generation was conducted following modified protocols reported in the literature [27,28]. Figure 1 schematically depicts the experimental setup used. All reactions were performed in a 50 mL three-neck round-bottom flask immersed in a thermostatic water bath maintained at 37 °C. The flask was equipped with a thermometer and connected via rubber tubing to a pneumatic trough for hydrogen collection using the water displacement method, with an inverted 50 mL water-filled burette serving as the gas-measuring device. Before each experiment, the gold-containing solution in the flask was purged with high-purity nitrogen (99.99 %) for 20 minutes at 80 mL/min to remove dissolved oxygen and establish an inert atmosphere [27,29]. Nitrogen was introduced through a submerged inlet needle while gently stirring the solution to enhance deaeration. After purging, the nitrogen inlet was closed and the system was immediately sealed to form a gas-tight setup consisting of the reaction

flask, connecting tubing, and inverted burette. A slight positive nitrogen headspace was maintained to minimize oxygen ingress, while the water in the inverted burette served as a liquid seal to prevent back-diffusion of air. The system was allowed to stabilize until the burette water level remained constant, confirming the absence of leaks, and establishing a stable baseline. The reaction was then initiated by introducing 8 g/L of nZVI/palm shell composites synthesised using different equimolar $NaBH_4$ and $FeCl_3$ concentrations (0.5-2 M) and a fixed amount of palm shell powder, as described in Section 2.2. The suspension was stirred at 300 rpm and allowed to react for 24 hours, during which hydrogen evolution was continuously collected and analysed via gas chromatography (GC-FID, Agilent Technologies) with nitrogen gas as a carrier gas to ascertain the hydrogen concentration in the gas mixture. After 1 minute of reaction, aliquots were withdrawn, and the magnetic nZVI/palm shell composites were separated using a magnet. The resulting supernatant containing nanogold colloids was filtered, rinsed, and analysed by UV-Vis spectroscopy to detect the LSPR peak in the 530 nm - 550 nm range.

3. Results and Discussion

This study examined how varying equimolar $NaBH_4$-$FeCl_3$ concentrations (0.5–2.0 M) influence the dual performance of nZVI/palm shell composites in simultaneous nanogold recovery and hydrogen generation. Although both processes started concurrently, nanogold reduction dominated initially due to its higher redox potential [17], while hydrogen generation occurred gradually over 24 hours, as discussed in the following sections with supporting UV-Vis and BET analyses.

3.1. Effect on Nanogold Recovery

Figure 2 shows the UV–Vis spectra of nanogold generated using nZVI/palm shell composites synthesised at varying equimolar $NaBH_4$–$FeCl_3$ concentrations (0.5–2.0 M). All spectra exhibit a well-defined localized surface plasmon resonance (LSPR) peak centered around

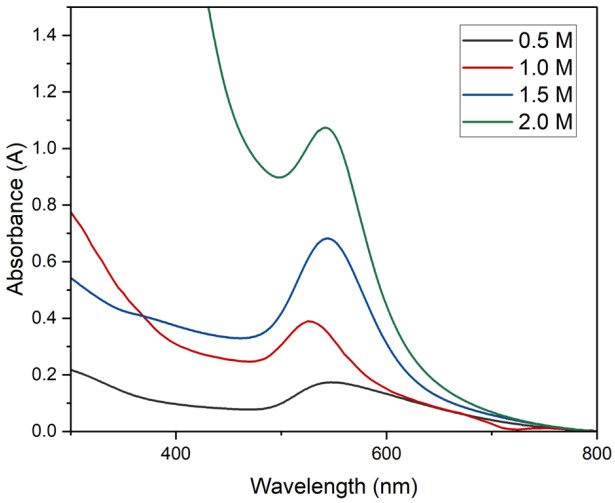

Figure 2. UV–Vis absorption spectra of nanogold recovered using nZVI/palm shell composites synthesized at varying equimolar $NaBH_4$–$FeCl_3$ concentrations.

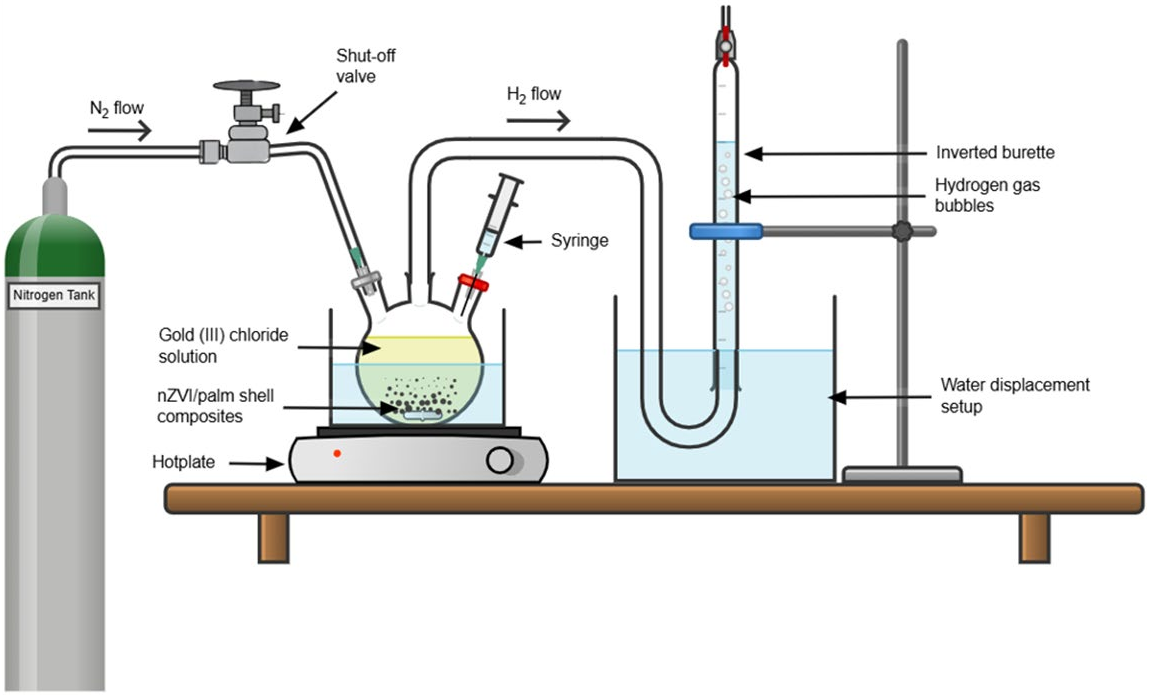

Figure 1. Experimental setup for simultaneous nanogold recovery and hydrogen generation using nZVI/palm shell composites.

530 nm, confirming the successful reduction of Au^{3+} to Au^0 by nZVI. The presence of a single, symmetrical LSPR peak indicates that the resulting AuNPs were predominantly spherical with a relatively narrow size distribution, consistent with typical spherical AuNPs absorbing in the 520–550 nm region [30,31]. The visible colour transition of the solution from light yellow to purple-red further corroborates AuNPs formation. Notably, the intensity of the LSPR peak increased systematically with precursor concentration, suggesting that the amount of nanogold produced is highly sensitive to the $NaBH_4$–$FeCl_3$ molarity used in composite synthesis.

This concentration-dependent behaviour is further quantified in Figure 3, which plots the average absorbance (used as a proxy for nanogold yield) as a function of the equimolar $NaBH_4$–$FeCl_3$ concentration. Absorbance values rose nearly linearly from 0.2227 A at 0.5 M to 1.0175 A at 2.0 M, demonstrating that higher precursor concentrations result in significantly greater nanogold recovery. This enhancement is likely associated with the increased availability of reactive Fe^0 sites generated in the composites at higher molarities, which may facilitate more rapid and extensive reduction of Au^{3+} to Au^0. The favourable redox potential gradient between Fe^0/Fe^{3+} (+0.33 V) and Au^{3+}/Au^0 (+1.50 V) further promotes efficient electron transfer [16,17], accelerating nanogold nucleation. As Fe^0 availability increases, a greater proportion of Au^{3+} ions undergo reduction, leading to higher LSPR intensities and greater nanogold formation. This trend is consistent with previous findings, such as those reported in a prior study [16], which also demonstrated improved Au^{3+} reduction efficiency with increasing iron precursor concentrations.

3.2. Effect on Hydrogen Volume

In this system, hydrogen generation occurs as nZVI within the nZVI/palm shell composites undergoes corrosion in aqueous environments, releasing electrons that reduce protons (H^+) or water molecules to produce hydrogen gas. The quantity and reactivity of the nZVI formed, both governed by the $NaBH_4$ and $FeCl_3$ concentrations used during composite synthesis, play a central role in determining the overall hydrogen output. As shown in Figure 4, the hydrogen volume exhibits a distinctly non-linear dependence on the equimolar $NaBH_4$–$FeCl_3$ concentrations, contrasting with the more linear trend observed for nanogold recovery profile (Figure 3).

At lower concentrations (0.5–1.0 M), hydrogen volume remained relatively stable (19.08–19.88 mL). Hydrogen generation increased substantially at 1.5 M, reaching 29.02 mL, before dropping sharply to 12.20 mL at 2.0 M. These results contrast with the continuous upward trend observed for nanogold recovery (Figure 3). The divergence arises from the different kinetics of the two redox processes: Au^{3+} reduction is rapid and dominates the early reaction period, whereas corrosion-driven hydrogen evolution proceeds more slowly over 24 hours. At 1.5 M, sufficient Fe^0 is available not only to fully reduce Au^{3+} but also to sustain long-term hydrogen evolution, resulting in the highest hydrogen volume. However, beyond 2.0 M, excessive precursor amounts produce larger quantities of nZVI, which accelerates Au^{3+} reduction but simultaneously leads to the rapid consumption of reactive Fe^0. Based on the observed reduction in hydrogen volume at higher concentrations, despite increasing nZVI availability, we infer that passivating layers of

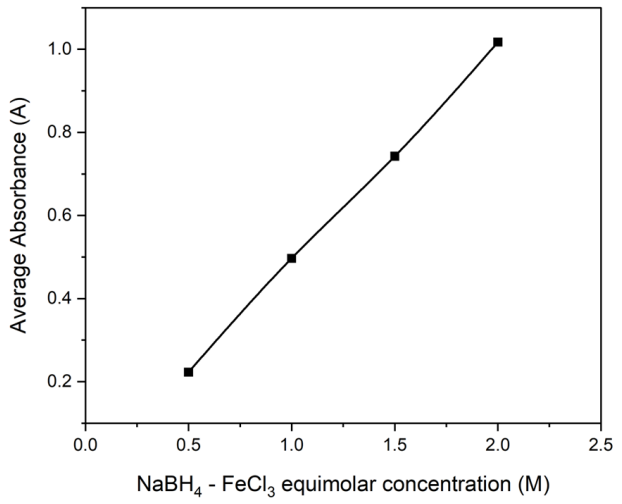

Figure 3. Average UV-Vis absorbance (proxy of nanogold yield) versus equimolar $NaBH_4$-$FeCl_3$ concentration for nZVI/palm shell composite synthesis.

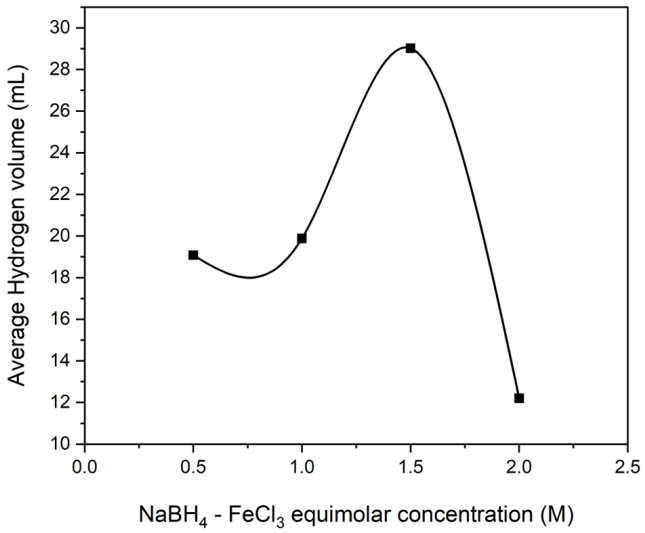

Figure 4. Average hydrogen volume versus equimolar $NaBH_4$-$FeCl_3$ concentration for nZVI/palm shell composite synthesis.

iron oxides/hydroxides may build on the nanoparticle surfaces, limiting electron transfer and suppressing long-term hydrogen production. Although no direct surface characterisation of passivation layers was conducted out in this study, this interpretation is compatible with the observed kinetic behaviour and with mechanistic models reported in the literature. Similar behaviour has been reported in the literature [12], where reduced long-term hydrogen generation was observed at higher nZVI dosages. Comparable trends were also reported in other studies [32,33], which attributed that hydrogen evolution decreased exponentially over time, consistent with progressive surface passivation by oxide/hydroxide layers that block access to the underlying Fe^0 and impede electron transfer, thereby reducing overall reactivity.

Although nanogold recovery continued to increase up to 2 M (Figure 3), hydrogen generation peaked at 1.5 M (Figure 4). This difference shows a fundamental trade-off in the system: increasing equimolar $NaBH_4$-$FeCl_3$ concentration speeds up the reduction of Au^{3+} ions, but it also slows down the long-term corrosion needed for hydrogen evolution. The reaction condition of 1.5 M therefore represents an optimal balance where both nanogold recovery and hydrogen production are jointly maximized, confirming the synergistic dual-function nature of the nZVI/palm shell composites.

3.3 Hydrogen Purity and Gas Composition

The evolved gas mixture was characterised by GC-FID to determine hydrogen purity and quantify the composition of gaseous products generated from the nZVI/palm shell system. Table 1 shows the concentrations of the gaseous species detected in the collected samples. As summarised in Table 1, hydrogen accounted for 99.88 mol% of the total detected gas, indicating that the nZVI/palm shell system predominantly produces hydrogen with negligible interference from other gaseous species. Only trace amounts of CO_2 (0.01 mol%) and CO (0.03 mol%) were detected, confirming minimal side reactions following correction for the blank response. This level of hydrogen purity is consistent with prior results from nZVI-based hydrogen production systems. For instance, hydrogen produced from a Bi/Fe^0 water system was reported to contain negligible levels of common gaseous impurities such as CO_2 and CH_4, highlighting its potential as a clean energy carrier [18]. Similarly, hydrogen formation arising from nZVI dissolution has been shown to correlate with minimal CO_2 generation under anaerobic conditions, indicating that nZVI itself can serve as a direct source of hydrogen in biomass-based systems [27]. Compared to previous findings, the present system has a high hydrogen purity, showing that the palm shell-supported nZVI promotes selective iron corrosion while inhibiting competing side reactions. This indicates that the nZVI/palm shell composites can produce high-purity hydrogen with little gaseous byproducts, highlighting their potential for clean and sustainable energy applications.

Table 1. Concentration of gases collected from nZVI/palm shell composites.

Total gas concentration (%mole)	Gas concentration (%mole)		
	H_2	CO_2	CO
14.28	99.88	0.01	0.03

3.4. BET Surface Area and Pore Size Analysis of nZVI/Palm Shell Composites

The specific surface area and pore size distribution of the nZVI/palm shell composites were evaluated using BET analysis, with the results shown in Figure 5. The composites exhibited the highest BET surface area (13.57 m^2/g) at an equimolar $NaBH_4$-$FeCl_3$ concentration of 1.5 M, while the largest pore size (217.77 Å) was observed at a concentration of 2.0 M. The increase in specific surface area from 8.69 m^2/g (0.5 M) to 13.57 m^2/g (1.5 M) is significant, as increased surface area enhances adsorptive interactions and redox activity of Fe^0 nanoparticles. This is consistent with the improved nanogold recovery and hydrogen production observed at 1.5 M (Figures 3 and 4), implying that this concentration generated an optimum composite microstructure with a high density of active Fe^0 sites.

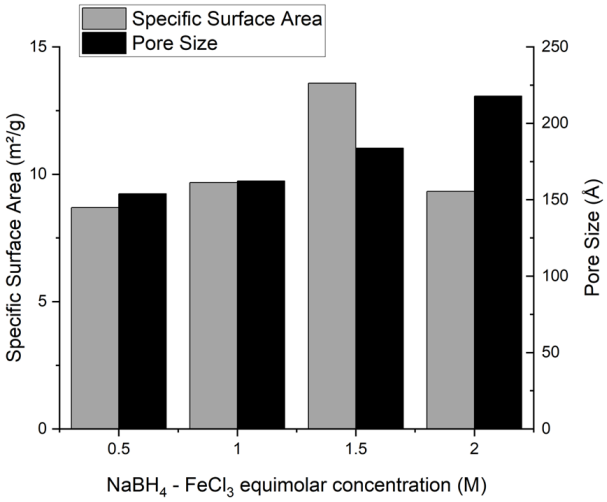

Figure 5. Specific surface area and pore size of nZVI/palm shell composites synthesized at varying equimolar $NaBH_4$–$FeCl_3$ concentrations.

At 2.0 M, however, although the pore size was the highest, the specific surface area decreased to 9.33 m^2/g. This suggests that excessively high $NaBH_4$ and $FeCl_3$ concentrations may cause pore coalescence or partial structural collapse, weakening the internal pore network. Under these conditions, the accelerated nucleation and growth of nZVI can produce larger agglomerates that combine and block nearby pores within the composites [34]. Although no direct microscopic or spectroscopic evidence of pore collapse or surface passivation was determined in this study, the reduction in BET surface area, together with the decrease in hydrogen evolution at 2.0 M (Figure 4), provides indirect evidence that structural densification and surface deactivation may occur at higher precursor concentrations. These structural alterations may limit prolonged redox activity by reducing the accessibility of Fe^0 surface sites and impeding effective electron transfer [35]. Similarly, the structural instability in nZVI composites at high precursor concentrations has been reported to result in poor textural properties and the formation of a passivating oxide layer that inhibits electron transfer and increased aggregation [34,36].

Overall, the BET results highlight those textural properties play a crucial role in determining Au^{3+} reduction and hydrogen generation efficiency. The nZVI/palm shell composites synthesized at 1.5 M exhibited a well-developed mesoporous structure that balances surface area for rapid nanogold recovery and structural stability for long-term hydrogen generation. These findings emphasize the importance of $NaBH_4$ and $FeCl_3$ concentration optimization to engineer surface characteristics that enhance multifunctional nanocomposite performance. Future research should utilize direct surface characterization techniques [36], and explore kinetics and thermodynamics of the sequential redox reactions between Fe^0, Au^{3+}, and water to identify rate-limiting steps and optimize overall performance, similar to other nanocomposite systems [37].

4. Conclusion

This study demonstrated the successful synthesis of palm shell-derived nZVI composites for simultaneous nanogold recovery and hydrogen generation from $HAuCl_4$ solutions. By varying equimolar $NaBH_4$–$FeCl_3$ concentrations, 1.5 M was identified as the optimal condition, producing composites with the highest BET surface area and a stable mesoporous structure. This balance of reactivity and structural integrity enabled rapid Au^{3+} reduction and sustained hydrogen evolution, with 1.5 M serving as the "sweet spot" that maximizes both nanogold recovery and hydrogen production. Using palm shell biomass as the support further enhanced the economic and environmental sustainability of the material. Overall, the findings highlight the potential of nZVI/palm shell composites as a multifunctional platform for wastewater treatment, precious metal recovery, and hydrogen-based energy applications.

Acknowledgment

The authors gratefully acknowledge the Ministry of Higher Education (MOHE), Malaysia, for financial support through the Fundamental Research Grant Scheme (FRGS/1/2023/TK08/UITM/02/5; FRGS/1/2022/TK08/UITM/02/10), as well as Universiti Teknologi MARA (UiTM) for additional support through the UiTM Conference Support Fund.

CRedit Author Statement

Author Contributions: P. N. S. Nordin: Conceptualization, Methodology, Investigation, Resources, Writing, Review and Editing, Visualization; A. S. N. Helmy: Methodology, Investigation, Resources; C. J. C. Derek: Resources, Funding acquisition; M. F. Rajuli: Resources, Funding acquisition; S. H. Chang: Validation, Review and Editing, Supervision, Project administration. All authors have read and agreed to the published version of the manuscript.

References

[1] Yeh, Y.C., Creran, B., Rotello, V.M. (2012). Gold nanoparticles: Preparation, properties, and applications in bionanotechnology. *Nanoscale* 4, 1871–1880. DOI: 10.1039/c1nr11188d.

[2] Chang, S., Jampang, A. (2023). Enhanced adsorption selectivity of Au(III) over Cu(II) from acidic chloride solutions by chitosan/palm kernel fatty acid distillate/magnetite nanocomposites. *International Journal of Biological Macromolecules*, 252, 126491. DOI: 10.1016/j.ijbiomac.2023.126491.

[3] Rao, M.D., Singh, K.K., Morrison, C.A., Love, J.B. (2020). Challenges and opportunities in the recovery of gold from electronic waste. *RSC Advances*, 10(8), 4300–4309. DOI: 10.1039/c9ra07607g.

[4] Sharma, R., Kim, Y., Lee, E., Lee, H. (2024). Ultrapure gold recovery from electronic waste as nanoparticles immobilized in hydrogel matrix. *Chemical Engineering Journal*, 499. DOI: 10.1016/j.cej.2024.156539.

[5] Wu, Y., Fang, Q., Yi, X., Liu, G., Li, R.W. (2017). Recovery of gold from hydrometallurgical leaching solution of electronic waste via spontaneous reduction by polyaniline. *Progress in Natural Science: Materials International*, 27(4), 514–519. DOI: 10.1016/j.pnsc.2017.06.009.

[6] Chang, S.H., Jampang, A.O.A. (2021). Green extraction of gold(III) and copper(II) from chloride media by palm kernel fatty acid distillate. *Journal of Water Process Engineering*, 43, 102298. DOI: 10.1016/j.jwpe.2021.102298.

[7] Halim, S.F.A., Chang, S.H., Morad, N. (2020). Extraction of Cu(II) ions from aqueous solutions by free fatty acid-rich oils as green extractants. *Journal of Water Process Engineering*, 33. DOI: 10.1016/j.jwpe.2019.100997.

[8] Chang, S.H. (2017). Parametric studies on an innovative waste vegetable oil-based continuous liquid membrane (WVCLM) for Cu(II) ion separation from aqueous solutions. *Journal of Industrial and Engineering Chemistry*, 50, 102–110. DOI: 10.1016/j.jiec.2017.01.037.

[9] Chang, S.H. (2018). A Comparative Study of Batch and Continuous Bulk Liquid Membranes in the Removal and Recovery of Cu(II) Ions from Wastewater. *Water, Air, & Soil Pollution*, 229(1), 22. DOI: 10.1007/s11270-017-3659-z.

[10] Chaurasia, A.K., Mondal, P. (2021). Hydrogen production from waste and renewable resources. In: *Hydrogen Fuel Cell Technology for Stationary Applications*. IGI Global, pp. 22–46. DOI: 10.4018/978-1-7998-4945-2.ch002.

[11] Chang, S.H., Rajuli, M.F. (2024). An overview of pure hydrogen production via electrolysis and hydrolysis. *International Journal of Hydrogen Energy*, 84, 521–538. DOI: 10.1016/j.ijhydene.2024.08.245.

[12] Chen, K.F., Li, S., Zhang, W.X. (2011). Renewable hydrogen generation by bimetallic zero valent iron nanoparticles. *Chemical Engineering Journal*, 170(2–3), 562–567. DOI: 10.1016/j.cej.2010.12.019.

[13] Cheng, Y., Dong, H., Hao, T. (2021). CaCO3 coated nanoscale zero-valent iron (nZVI) for the removal of chromium(VI) in aqueous solution. *Separation and Purification Technology*, 257 DOI: 10.1016/j.seppur.2020.117967.

[14] Ling, L., Huang, X.Y., Zhang, W.X. (2018). Enrichment of Precious Metals from Wastewater with Core–Shell Nanoparticles of Iron. *Advanced Materials*, 30(17). DOI: 10.1002/adma.201705703.

[15] Han, L., yang, L., Wang, H., Hu, X., Chen, Z., Hu, C. (2016). Sustaining reactivity of Fe0 for nitrate reduction via electron transfer between dissolved Fe2+ and surface iron oxides. *Journal of Hazardous Materials*, 308, 208–215. DOI: 10.1016/j.jhazmat.2016.01.047.

[16] Djafari, J., Fernández-Lodeiro, A., García-Lojo, D., Fernández-Lodeiro, J., Rodríguez-González, B., Pastoriza-Santos, I., Pérez-Juste, J., Capelo, J.L., Lodeiro, C. (2019). Iron(II) as a Green Reducing Agent in Gold Nanoparticle Synthesis. *ACS Sustainable Chemistry and Engineering*, 7(9), 8295–8302. DOI: 10.1021/acssuschemeng.8b06690.

[17] Li, S., Li, J., Wang, W., Zhang, W. xian (2019). Recovery of gold from wastewater using nanoscale zero-valent iron. *Environmental Science: Nano*, 6(2), 519–527. DOI: 10.1039/C8EN01018H.

[18] Sayed, M., Khan, A., Rauf, S., Shah, N.S., Rehman, F., A. Al-Kahtani, A., Khan, J.A., Iqbal, J., Boczkaj, G., Gul, I., Bushra, M. (2020). Bismuth-Doped Nano Zerovalent Iron: A Novel Catalyst for Chloramphenicol Degradation and Hydrogen Production. *ACS Omega*, 5(47), 30610–30624. DOI: 10.1021/acsomega.0c04574.

[19] Aminu, I., Nahil, M.A., Williams, P.T. (2020). Hydrogen from Waste Plastics by Two-Stage Pyrolysis/Low-Temperature Plasma Catalytic Processing. *Energy and Fuels*, 34(9), 11679–11689. DOI: 10.1021/acs.energyfuels.0c02043.

[20] Han, Y., Yang, M.D.Y., Zhang, W., Yan, W. (2015). Optimizing synthesis conditions of nanoscale zero-valent iron (nZVI) through aqueous reactivity assessment. *Frontiers of Environmental Science and Engineering*, 9(5), 813–822. DOI: 10.1007/s11783-015-0784-z.

[21] Liou, Y.H., Lo, S.L., Kuan, W.H., Lin, C.J., Weng, S.C. (2006). Effect of precursor concentration on the characteristics of nanoscale zerovalent iron and its reactivity of nitrate. *Water Research*, 40(13), 2485–2492. DOI: 10.1016/j.watres.2006.04.048.

[22] Turabik, M., Simsek, U. (2017). Effect of synthesis parameters on the particle size of the zero valent iron particles. *Synthesis and Reactivity in Inorganic Metal-Organic and Nano-Metal Chemistry*, 47, 1033–1043. DOI: 10.1080/15533174.2016.1219869.

[23] Eljamal, R., Eljamal, O., Khalil, A.M., Aljamal, R., Khalil, A., Saha, B.B., Matsunaga, N. (2017). Effects of sodium borohydride as a reductant on the synthesis of Nano-scale zero-valent iron. *Proceedings of International Exchange and Innovation Conference on Engineering & Sciences (IEICES)*, 39–42. DOI: 10.15017/1906152

[24] Yusuf, S.A., Ismail, S.N.S., Zubairi, M.S.R.M.A., Muthuraman, G., Halim, S.F.A., Chang, S.H. (2025). Hydrogen Production by Formic Acid Decomposition with Nanoscale Zero-Valent Iron (nZVI): Effects of nZVI Dosage, Temperature and Time. *Journal of Advanced Research in Fluid Mechanics and Thermal Sciences*, 125(1), 158–166. DOI: 10.37934/arfmts.125.1.158166.

[25] Prasetyo, I., Mukti, N.I.F., Cahyono, R.B., Prasetya, A., Ariyanto, T. (2020). Nanoporous Carbon Prepared from Palm Kernel Shell for CO2/CH4 Separation. *Waste and Biomass Valorization*, 11(10), 5599–5606. DOI: 10.1007/s12649-020-01006-4.

[26] Singh, A.K., Rarotra, S., Pasumarthi, V., Mandal, T.K., Bandyopadhyay, D. (2018). Formic acid powered reusable autonomous ferrobots for efficient hydrogen generation under ambient conditions. *Journal of Materials Chemistry A*, 6(19), 9209–9219. DOI: 10.1039/c8ta02205d.

[27] Huang, Y.X., Guo, J., Zhang, C., Hu, Z. (2016). Hydrogen production from the dissolution of nano zero valent iron and its effect on anaerobic digestion. *Water Research*, 88, 475–480. DOI: 10.1016/j.watres.2015.10.028.

[28] Li, P., Lv, F., Xu, J., Yang, K., Lin, D. (2021). Separation and Analysis of Nanoscale Zero-Valent Iron from Soil. *Analytical Chemistry*, 93(29), 10187–10195. DOI: 10.1021/acs.analchem.1c01452.

[29] Yang, Y., Guo, J., Hu, Z. (2013). Impact of nano zero valent iron (NZVI) on methanogenic activity and population dynamics in anaerobic digestion. *Water Research*, 47(17), 6790–6800. DOI: 10.1016/j.watres.2013.09.012.

[30] Panda, B.R., Chattopadhyay, A. (2007). Synthesis of Au nanoparticles at "all" pH by H2O2 reduction of HAuCl4. *Journal of Nanoscience and Nanotechnology*. 1911–1915. DOI: 10.1166/jnn.2007.740.

[31] El Mitwalli, O.S., Barakat, O.A., Daoud, R.M., Akhtar, S., Henari, F.Z. (2020). Green synthesis of gold nanoparticles using cinnamon bark extract, characterization, and fluorescence activity in Au/eosin Y assemblies. *Journal of Nanoparticle Research*, 22(10). DOI: 10.1007/s11051-020-04983-8.

[32] Liu, A., Liu, J., Han, J., Zhang, W.-X. (2015). Evolution of Nanoscale Zero-valent Iron (nZVI). Water: Microscopic and Spectroscopic Evidence on the Formation of Nano-and Micro-structured Iron Oxides. *Journal of Hazardous Materials*, 322, 129–135. DOI: 10.1016/j.jhazmat.2015.12.070

[33] Zhao, Z., Qiu, Y., Lei, B., Zhang, C., Liu, Z., Wang, W., Wang, H., Li, T. (2025). Amorphous Nano Zero-Valent Iron (A-nZVI) Modified by Ethylenediamine for Efficient Dechlorination of Trichloroethylene: Structure, Kinetics, and Mechanism. *Catalysts*, 15(12). DOI: 10.3390/catal15121173.

[34] Hwang, Y.H., Kim, D.G., Shin, H.S. (2011). Effects of synthesis conditions on the characteristics and reactivity of nano scale zero valent iron. *Applied Catalysis B: Environmental*, 105(1–2), 144–150. DOI: 10.1016/j.apcatb.2011.04.005.

[35] Bae, S., Collins, R.N., Waite, T.D., Hanna, K. (2018). Advances in Surface Passivation of Nanoscale Zerovalent Iron: A Critical Review. *Environmental Science and Technology*, 52(21), 12010–12025. DOI: 10.1021/acs.est.8b01734.

[36] Pang, H., Zhang, E., Zhang, D., Wang, X., Zhao, B., Liu, L., Ma, X., Song, G., Yu, S. (2022). Precursor impact and mechanism analysis of uranium elimination by biochar supported sulfurized nanoscale zero-valent iron. *Journal of Environmental Chemical Engineering,* 10(2) DOI: 10.1016/j.jece.2022.107288.

[37] Chang, S.H., Jampang, A.O.A., Din, A.T.M. (2025). Adsorption isotherms, kinetics, and thermodynamics of Au(III) on chitosan/palm kernel fatty acid distillate/magnetite nanocomposites. *International Journal of Biological Macromolecules*, 304, 140913. DOI: 10.1016/j.ijbiomac.2025.140913.